Differential Phosphorylation and N-terminal Configuration of Capsid Subunits in Parvovirus Assembly and Viral Trafficking

Jon Gil-Ranedo[1], Eva Hernando[2], Noelia Valle[3], Laura Riolobos[4], Beatriz Maroto[5],

and José M. Almendral[#]

Centro de Biología Molecular "Severo Ochoa" (Consejo Superior de Investigaciones Científicas-Universidad Autónoma de Madrid), Cantoblanco, 28049 Madrid, Spain.

Running Title: Structural proteins phosphorylation in parvovirus assembly and traffic

Present address: [1]Peninsula School of Medicine, Plymouth University, PL6 8BU Plymouth, UK; [2]Department of Pathology, NYU Cancer Center, NY10016, USA; [3]Departamento de Biotecnología, Universidad Francisco de Vitoria, Madrid, Spain; [4]Cancer Vaccine Institute, Center for Translational Medicine in Women's Health, University of Washington, Seattle, WA 98109, USA.; [5]NIMGenetics, PCM, 28049 Cantoblanco, Madrid, Spain.

[#]Corresponding author. Mailing address: José M. Almendral. Centro de Biología Molecular "Severo Ochoa" (CSIC-UAM). Universidad Autónoma de Madrid. Cantoblanco, 28049 Madrid. Spain. Phone: 34-91-1964559. Electronic mail address: jmalmendral@cbm.csic.es.

Abstract

The T1 parvovirus Minute Virus of Mice (MVM) was used to study the roles that phosphorylation and N-terminal domains (Nt) configuration of capsid subunits may play in icosahedral nuclear viruses assembly. In synchronous MVM infection, capsid subunits newly assembled as two types of cytoplasmic trimeric intermediates (3VP2, and 1VP1:2VP2) harbored a VP1 phosphorylation level fivefold higher than that of VP2, and hidden Nt. Upon nuclear translocation at S phase, VP1-Nt became exposed in the heterotrimer and subsequent subviral assembly intermediates. Empty capsid subunits showed a phosphorylation level restored to VP1:VP2 stoichiometry, and the Nt concealed in their interior. However ssDNA-filled virus maturing at S/G2 lacked VP1 phosphorylation and one major VP2 phosphopeptide, and exposed VP2-Nt. Endosomal VP2-Nt cleavage resulted in VP3 subunits devoid of any phospholabel, implying that incoming viral particles specifically harbor a low phosphorylation status. Phosphorylation provides a mechanistic coupling of parvovirus nuclear assembly to the cell cycle.

Keywords: Parvovirus/capsid phosphorylation/Nt configuration/assembly/maturation/viral trafficking

Introduction

In eukaryotes, the activity of protein kinases contributes to many fundamental processes such as signal transduction, metabolism, and the cell cycle, by catalyzing the transfer of negatively charged phosphoryl moieties predominantly to serine, threonine, and tyrosine amino acid residues (Manning *et al*., 2002; Ubersax and Ferrell, 2007). Viral proteins may serve as substrates for cellular or virus-encoded protein kinases, their phosphorylation influencing structure and function through conformational changes or direct chemical effects on protein interactions. Understanding the biological effect of phosphate substituents incorporated in virus structural proteins is challenged by their transient nature, technical difficulty to precisely map phosphorylation sites, and the lack of resolution in the 3-D structure of virus particles. Nevertheless phosphorylation of structural proteins of RNA and DNA viruses mediates processes key to their life cycles, such as recognition of cellular factors, assembly of viral components, genome packaging, or viral trafficking (e.g. Sugai *et al.,* 2014; Mondal *et al.,* 2015; Bjorn-Patrick and Roy, 2016; Zhang *et al*., 2016), and may provide targets for antiviral therapies. Icosahedral DNA animal viruses (such as *Herpesviridae, Adenoviridae, Papillomaviridae, Polyomaviridae, or Parvoviridae*) whose structural components must traffick through the nuclear envelope to assemble and mature, conform a framework of viral systems to explore the diversity of functions played by capsid proteins phosphorylation.

With the aim of constructing a comprehensive virus model on this issue, we chose the *Protoparvovirus* Minute Virus of Mice (MVM), a reference member of the *Parvoviridae* (Cotmore *et al*., 2014), and an important mouse pathogen (Brownstein *et al.,* 1991;

Ramirez *et al.,* 1996; Segovia *et al.,* 1999). Parvoviruses are nonenveloped eukaryotic nuclear viruses containing a 5kb single-stranded (ss) DNA genome in a 25 nm-diameter icosahedral (T=1) capsid made from two to three polypeptides. The MVM capsid is composed of about ten subunits of the VP1 (83 kDa) and fifty subunits of the VP2 (64 kDa) proteins (Cotmore and Tattersall, 2014). The 3-D atomic structure of the capsid resolved for many parvoviruses exhibits a common folding of the protein subunits in an eight-stranded antiparallel β-barrel topology, whereas the capsid surface may differ drastically due to prominent loops and depressions which confer characteristic functions (Tsao *et al*., 1991; Agbandje-McKenna *et al*., 1998; Xie *et al*., 2002; Kaufmann *et al*., 2004; Kontou *et al*., 2005; Gurda *et al*., 2010). The N-terminal (Nt) sequences of the parvovirus capsid proteins (VPs) are flexible sequences with generally unresolved structure in the crystals, with the exception of Nt of the human B19 major capsid protein (Kaufmann *et al*., 2008). However these unordered Nt can be alternatively exposed on the surface of the capsid in controlled processes to serve as trafficking signals at different stages of the viral life cyle (Maroto *et al*., 2004; Valle *et al*., 2006). The unique VP1 Nt sequence (1Nt) contains diverse protein motifs required by the incoming virus to initiate infection, such as phospholipase A2 (PLA_2) activity (Zadori *et al*., 2001; Farr *et al*., 2005), nuclear localization sequences (NLS) (Vihinen-Ranta *et al*., 2002; Lombardo *et al*., 2002; Sonntang *et al*., 2006; Johnson *et al*., 2010; Boisvert *et al*., 2014), and other functionally uncharacterized domains (Tullis *et al*., 1993; Lombardo *et al.,* 2002; Popa-Wagner *et al*., 2012; Porwal *et al*., 2013). The VP2 Nt sequence (2Nt) localized in the interior of empty capsids can be externalized by heat *in vitro* (Hernando *et al*., 2000; Carreira *et al*., 2004; Riolobos *et al*., 2010), but in DNA-filled virions some 2Nt are projected outside the capsid

(Cotmore and Tatersall, 2007; Plevka *et al.,* 2011; Subramanian *et al.,* 2017) presumably through the fivefold cylinder (Tsao *et al*., 1991; Agbandje-McKenna *et al*., 1998). The 2Nt serves as a signal for active nuclear export of mature MVM prior to cell destruction, an activity that may be crucial for successful viral dissemination in tissues (Maroto *et al*., 2004). Additionally, although devoid of recognized import signals, some intracellular exposure-competent 2Nt are required for the incoming virus to initiate infection (Sánchez-Martínez *et al*., 2012; Castellanos *et al*., 2013). 2Nt externalization presumably enlarges the capsid pore in the endosome (Sánchez-Martínez *et al.,* 2012), facilitating its cleavage-off VP2 subunits observed in the pH-dependent entry pathway of many parvoviruses (Tullis *et al*., 1992; Mani *et al*., 2006; Boisvert *et al.,* 2010; Parrish *et al*., 2010), a dynamic process leading to 1Nt externalization (Cotmore *et al*., 1999; Farr *et al*., 2006; Cotmore and Tatersall, 2014; reviewed in Ros *et al.,* 2017).

In productively infected cells, parvovirus capsid assembly takes place in the nucleus (Hoque *et al.,* 1999; Lombardo *et al.,* 2000), involving orchestrated interactions among capsid subunits. In MVM, assembly begins with the formation of two trimeric intermediates in the cytoplasm at stoichiometric amounts, a homotrimer (3VP2) and a heterotrimer (1VP1/2VP2) (Riolobos *et al*., 2006). Isolated trimers were nuclear transport competent in permeabilized cells without any other viral component (Riolobos et al., 2010; Gil-Ranedo *et al*., 2015). Trimers are translocated into the nucleus driven by a structured protein motif (NLM) displaced on the inner capsid surface as an amphipathic beta-strand (Lombardo *et al*., 2000). Similar non-conventional nuclear transport sequences localized in partially overlapping or contiguous homologous amino acid sequence of the NLM (Valle *et al*., 2006), were required for nuclear capsid assembly of the human B19 (Pillet *et al*., 2003), and porcine PPV (Boisvert *et al*., 2014) parvoviruses. These structured transport motifs may constitute a quality control

mechanism for the assembly pathway, precluding the nuclear import and assembly of misfolded subunits or trimers with unbalanced VP1 content (Lombardo *et al*., 2000). Within the nucleus, the MVM trimers interact through a few residues via hydrophobic and hydrogen bonds (Reguera *et al*., 2004), and must undergo conformational rearrangements to their final configuration in the capsid (Riolobos *et al.,* 2006 and 2010). In AAV2, an assembly-activating protein (AAP) encoded by the viral cap gene was essential for capsid assembly (Sonntag *et al*., 2010) presumably adapting the conformation of the VP subunits (Naumer *et al*., 2012).

The steps of the parvovirus life cycle (gene expression, nuclear translocation of proteins, capsid assembly, genome replication and encapsidation) are tightly coupled to the host cell cycle progression (Gil-Ranedo *et al.,* 2015). Importantly, parvovirus MVM gene expression in synchronous infection occurred at G1/S, implying that transcription does not require a previous viral DNA amplification, which indeed occurred later at S/G2 phase (Gil-Ranedo *et al.,* 2015). Capsid formation is particularly sensitive to cell cycle regulation, which is exerted at the level of non-conventional nuclear transport route(s) accessed by the assembly intermediates (Gil-Ranedo *et al.,* 2015). The coupling of parvovirus assembly to the cell cycle may largely rely on control of capsid subunits phosphorylation. In MVM infection, VP1 and VP2 structural subunits assembled into empty capsids were post-translationally modified through a complex and VP-specific pattern of phosphoserine and phosphothreonine residues (Maroto *et al*., 2000). The 3-D structure of virus-like particles (VLPs) lacking phosphorylation (Hernando *et al.,* 2000; Riolobos *et al*., 2010) that assembled in the cytoplasm (Riolobos *et al*., 2010; Yuan and Parris, 2001) indicated that, at least for the VP2-only capsid, subunit phosphorylation is not important for icosahedral T=1

ordering. However, nuclear transport of the VP2 homotrimer requires cytoplasmic phosphorylation by the Raf-1 kinase (Riolobos *et al,* 2010), although this phosphorylation was not sufficient to explain its cell cycle-regulated transport (Gil-Ranedo *et al*., 2015). Raf-1 phosphorylation targets serine residues of 2Nt (Maroto *et al*., 2000 and 2004), but localization of the many other phosphorylation sites in the VP1 and VP2 capsid subunits and their functions in the steps of the viral life cycle are unknown.

In this report, we have further investigated the phosphorylation and Nt configuration of the MVM structural proteins found in assembly intermediates and viral particles. Our focus was mainly on the less-studied VP1 subunits and their involvement in cell cycle-dependent VPs nuclear transport, capsid assembly, and MVM genome packaging. We show that VP1 subunits are hyperphosphorylated in cytoplasmic assembly intermediates, but are subjected to an orchestrated dephosphorylation programme during assembly that correlates with changes in Nt configuration. Furthermore, empty and DNA-filled virus particles drastically differed in the phosphorylation status of their VP1 and VP2 protein subunits. These data are integrated into an assembly and viral trafficking unified model of potential general interest to understand the life cycle of icosahedral nuclear viruses.

Materials and Methods

Virus and cell culture.

The prototype (p) strain of the *Protoparvovirus* Minute Virus of Mice (MVMp; Crawford, 1966) was used in this study and referred as MVM. The NB324K simian virus 40-transformed human newborn kidney cell line highly susceptible to the MVM strains (Gardiner and Tattersall, 1983), and a constitutively VPs-expressing stably transfected clone (Gil-Ranedo *et al.,* 2015), were maintained under minimal number of passages in Dulbecco Modified Eagle Medium (DMEM) supplemented with 5% heat-inactivated foetal calf serum (FCS; Gibco BRL). Wherever indicated in the text, infected or transfected cells were synchronized at G1/S with the DNA polymerase-α antagonist aphidicolin, or at G1 upon transfection by density arrest, as described (Gil-Ranedo *et al.,* 2015). Viral stocks used for infections were prepared from large-scale transfection using the pMM984 infectious plasmid (Tattersall and Bratton, 1983), and purified devoid of empty capsids as described (Sánchez-Martínez *et al*., 2012). Infectious virus titers and reliable plaque sizes were obtained by optimizing previously described plaque assay methods (Tattersall and Bratton, 1983; Rubio *et al*., 2005) as follows. NB324K cells were dispersed by carefully flushing three times through a 22G needle, and seeded at a density of $2x10^5$ cells/P60mm dish. Virus dilutions and cell inoculation (0.25 ml of virus sample per P60mm dish) were performed the next day in complete PBS supplemented with 0.1% FCS. After virus adsorption (1 h at 37 ºC under constant shaking) cells were overlaid with 7 ml/P60mm dish of a freshly prepared media composed of DMEM, 10 % FCS, non-essential amino acids, and 0.7% low melting agarose (SeaPlaque™ Lonza, prepared in ddH_2O). Plaques were developed six days afterwards by

fixing with 10% formaldehyde, and staining with 0.1 % crystal violet prepared in 4 % formaldehyde.

Flow cytometry.

Cell were fixed, permeabilized, and stained for viral antigens expression and DNA content as described (Gil-Ranedo *et al*., 2015). Samples were analyzed in a BD Biosciences FACSCanto II Flow Cytometer with the BD FACSDiva (v6.1.2, BD Biosciences) and FlowJo (v9.3 TreeStar) softwares.

Plasmids.

A non-replicative genomic clone of the MVMp viral strain (Ramirez et al., 1995; pMVM.WT), and the pMVM.VP1-only and pMVM.VP2-only derived genomic clones constructed by cDNA cloning allowing single expression of each of the structural proteins (Sánchez-Martínez *et al*., 2012), were used in cell transfections. Other plasmids were the pSVtk-VPs expressing the VP1 and VP2 capsid proteins of MVMp (Ramirez *et al*., 1995), and the pSVtk-VPs K153A and pSVtk-VPs L565W plasmids carrying single mutations in the common sequence of both structural proteins (Reguera *et al.,* 2004) that impaired capsid assembly (Riolobos *et al*., 2006).

Production of purified radiolabeled viral particles.

^{32}P-labeled empty capsids and DNA-filled viral particles of MVMp were produced and purified in NB324K cells following a previously described method (Maroto *et al*., 2000; Santarén *et al.,* 1993) with some modifications. Cells were infected at MOI 10, starved for 4 h in phosphate-free DMEM supplemented with 5 % dialyzed FCS, and labeled from 4 to 42 hpi

in the same medium containing 0.5 mCi per ml of [^{32}P]orthophosphate carrier free (Amersham). Cultures were scraped into the medium supplemented with 0.2 % sodium dodecyl sulphate (SDS), proteases (1mM phenylmethylsulfonyl fluoride (PMSF); 10 μg/ml aprotinin; 10 μg/ml pepstatin; 10 μg/ml leupeptine) and phosphatases (5 mM NaF, 20 mM β-glycerophosphate) inhibitors, clumps disaggregated by gentle sonication, and debris removed by low speed centrifugation (10,000 x g, 15 min). Homogenates were centrifuged at 15 °C and 30,000 x g for 18 h in a Sorvall AH627 rotor, through two volumes of a 20 % sucrose cushion in 50 mM Tris pH 7.5, 50 mM NaCl, 1 mM EDTA, and 0.2 % SDS. Pellets were resuspended in 1 ml per 90 mm dish of 20 mM Tris-HCl pH 7.5, 1 mM EDTA, 0.2 % Sarkosyl, and the proteases and phosphatases inhibitors as above, the suspensions adjusted to a density of 1.38 g/ml in CsCl by refractometry, and centrifuged to equilibrium at 150,000 x g for 24 h and 12 °C in a Sorvall TFT 80.13 rotor. Fractions with a density corresponding to empty capsids (1.32 g/ml), and DNA-full virus (1.39-1.41 g/ml), were pooled apart and centrifuged again at the same conditions. The ^{32}P-label distribution in the second round of gradients was determined by scintillation counting, fractions of empty and DNA-filled virus extensively dialyzed against PBS, and finally concentrated by ultracentrifugation at 100,000x g and 4 ºC for 6 h in a SW 40Ti Beckman rotor.

To fairly determine the phosphorylation level of the MVM capsid subunits in the viral particles (Fig. 5), SDS-PAGE gels containing resolved proteins of purified ^{32}P-labeled empty capsids and DNA-filled virus were equilibrated at room temperature for 15 min in twenty gel-volumes of 20 mM Tris-HCl pH 7.5, 10 mM $MgCl_2$, 5 mM NaCl, and then incubated in two gel-volumes with 10 U/ml of DNase I (Promega) for 30 min at 37 ºC under shaking. The gel was finally fixed in methanol-acetic, dried under vacuum, and exposed for autoradiography to X-ray films.

Antibodies

A collection of rabbit and mouse antibodies was used to specifically identify MVM capsid proteins, which included: a rabbit antiserum recognizing unassembled VP1 and VP2 subunits (α-VPs; Gil-Ranedo *et al.,* 2015); a mouse monoclonal antibody recognizing a structured epitope conformed at the 3x axis of the MVM capsid (α-Capsid, B7-MAb; López-Bueno *et al*., 2003; Kaufmann et al., 2007) but failing to react with unassembled or VP trimeric assembly intermediates (Riolobos et al., 2006; 2010); a rabbit antiserum raised against a 2Nt peptide that recognized mature DNA-filled virus (Maroto *et al.,* 2004); a rabbit antiserum raised against an expressed 1Nt peptide (Cotmore *et al*., 1999); and a mouse antiserum raised against denatured VP2 purified by SDS-PAGE following a previously described methodology (Gil-Ranedo *et al*., 2015), which was used for double immunofluorescence in combination with the rabbit α-2Nt and α-1Nt antibodies (α-VPs, Fig. 2 to 4).

Immunological analyses.

Double-labeled indirect immunofluorescence (IF) was performed in cells fixed with 4% paraformaldehyde buffered at pH 7.0 following previously described methods (Gil-Ranedo *et al*., 2015; Lombardo *et al.,* 2002; Maroto *et al*., 2004). Phenotypes were visualized by epifluorescence in a Zeiss Axiovert2000 inverted microscope coupled to a SPOT RT Slider digital camera and MetaVue 5.07 software, and images were taken in a Zeiss LSM 710 Laser Scanning confocal microscope and ZEN 2008 software. For western-blot analysis, protein samples resolved in 8 % SDS-PAGE and electro-blotted to nitrocellulose membranes were probed with the indicated antisera, developed with chemiluminescence (Thermo scientific), and exposure to X-ray films.

Isolation of radiolabeled assemblies.

NB324K cells stably expressing VPs proteins were arrested at G1/S by isoleucine deprivation and aphidicolin as described (Gil-Ranedo *et al*., 2015), and labeled for 4 h within the arrest with 200 μCi/ml of ^{35}S-methionine (Pro-mix^{TM}, Amersham) in methionine-free medium, or with 2 mCi/ml of carrier-free ^{32}P-orthophosphate (Amersham) in phosphate-free medium. At the end of the labelling periods cells were detached with trypsin and disrupted in 50 mM Tris-HCl pH 7.5, 10 mM NaCl in a cooled water bath sonicator. Lysates cleared by centrifugation at 15000 x g and 4 °C for 15 min in a bench-top centrifuge were subjected to immune-precipitation with the indicated antibodies bound to protein A-Sepharose in 50 mM Tris-HCl pH 7.5, 10 mM NaCl and proteases and phosphatase inhibitors (Calbiochem; Riolobos *et al*., 2010), under native (0.1 % Nonidet P-40) or denaturing (0.5 % SDS) conditions, and the precipitated boiled in Laemmli buffer prior SDS-PAGE and autoradiography.

2D phosphopeptides analysis.

A previously described methodology was followed (Maroto et al., 2000; Riolobos *et al*., 2010). In brief, the structural proteins of ^{32}P-radiolabelled purified empty capsids and DNA-filled viral particles were resolved by 8 % SDS-PAGE, blotted to nitrocellulose membranes, and exposed for autoradiography. The phospho-labelled VP1 and VP2 proteins were cut-off from the membranes and subjected to 2-D tryptic phosphopeptide analysis by digestion with N-tosyl-L-phenylalanine chloromethyl ketone (TPCK)-trypsin (sequencing grade, Boehringer). The resulting phosphopeptides were 2-D resolved in 20x20 cm TLC plates (Merck, Darmstadt, Germany), and the plates exposed to a radioanalytic imaging system (Fujix BAS 1000, Fuji) for

the indicated periods of time. The optical densities of the recorded phosphopeptide spots, as well as the phosphoprotein bands obtained in the autoradiography films, were determined with a GS-900™-Calibrated Densitometer (Bio-RadLaboratories, Hercules, California, USA).

Results

The protein subunits of MVM trimeric capsid assembly intermediates are unevenly phosphorylated.

At early stages of the MVM assembly pathway, the S phase-coupled nuclear translocation of trimeric intermediates required VPs phosphorylation by Raf-1 (Riolobos *et al.,* 2010), although a significant change in the VP2 phosphorylation pattern between quiescent and proliferating cells was not evident (Gil-Ranedo *et al.,* 2015). To analyze a possible role of VP1 phosphorylation in this process, the VP1/VP2 phosphorylation ratio in the trimers was studied prior to nuclear transport. We used VPs-expressing transfected human NB324K cells, which harboured high Raf-1 constitutive activity (Riolobos *et al*., 2010) and cell cycle dependent VPs transport as happens in infection (Gil-Ranedo *et al.,* 2015). The subcellular distribution of VPs subunits (Fig. 1A) either during growth, arrested at G1/S, or released from the arrest, was consistent with the previously described cell cycle dependence (Gil-Ranedo *et al.,* 2015). Therefore, synchronized cells at G1/S showing VPs retained in the cytoplasm (Fig. 1A, middle panel) were labeled during the arrest with ^{35}S-Met or with ^{32}P-orthophosphate, cell extracts immunoprecipitated with antibodies recognizing the 1Nt (α-VP1 antibody), or total unfolded VPs subunits (α-VPs antibody) under native or denaturing conditions (see Materials and Methods), and subjected to SDS-PAGE and autoradiography. Whereas denaturing conditions probed the specificity of the antibodies (Fig. 1B, d lanes), immunoprecipitation in native conditions of the ^{35}S-labeled samples showed a 1:5 ratio of VP1:VP2 subunits in the assemblies, their approximate stoichiometry of synthesis (Riolobos *et al*., 2006), when using the α-VPs antibody, but a ratio close to 1:2 when the α-VP1 antibody was used (Fig. 1B, n lanes; Fig. 1C). This

result indicated that the VP1 subunits assemble into a cytoplasmic 1VP1:2VP2 heterotrimer in G1/S arrested cells. The ^{32}P-labeled immunoprecipitates showed that newly synthesized VP1 and VP2 proteins accumulating in the cytoplasm were phosphorylated (Fig. 1B, d lanes). Importantly, the denaturing conditions of immunoprecipitation allowed resolution of the phosphorylated proteins at a VP1:VP2 ratio close to 1.0 (Fig. 1B, C). In respect to their ratio of synthesis shown above, this result indicated that, on average, VP1 subunits assembled in cytoplasmic trimers harbored a phosphorylation level close to fivefold higher than that of the VP2 subunits. Whether the VP2 subunits assembled in homo- (3VP2) and the hetero- (1VP1/2VP2) trimers differed in phosphorylation level could not be discerned.

Exposure of VP N-terminal domains in cytoplasmic assembly intermediates.

To get further insights into MVM assembly, we assessed changes in the configuration of the capsid subunits throughout the process by testing the accessibility of the VP1 (1Nt) and VP2 (2Nt) N-terminal domains to specific antibodies in cytoplasmic and nuclear assembly intermediates. It was previously shown that nuclear transport of VPs in transfected and infected NB324K cells was inhibited when subjected to density arrest contacts by a VP2-driven mechanism (Gil-Ranedo *et al.,* 2015). We therefore studied whether the Nt domains, carrying transport signals (see above), may contribute to this cell cycle-dependent mechanism. For this, we used a viral genomic plasmid (pMVM), and derived genomic constructs lacking either VP1 or VP2 (Sanchez-Martinez *et al.,* 2012), in transfections under different culture conditions. In pMVM transfections, the 1Nt domain was stained only in the nucleus under normal low cell density, but not in cells showing a cytoplasmic or mixed VPs transport phenotype at high density (Fig. 2 upper panels). In the absence of VP2 subunits though (pMVMVP1-only transfections), the 1Nt domain was efficiently

stained in the nucleus of cells grown to low and high density (Fig. 2, bottom panels). The 2Nt domain became similarly accessible to specific antibodies in the nucleus of pMVM and pMVMVP2-only transfected cells cultured at low density, denoting the production of DNA-filled viral particles, but not in singly expressed nuclear VP1 subunits albeit they contain the 2Nt amino acids sequence (Fig. 2, left panels). However, 2Nt was hidden when pMVM and pMVMVP2-only transfected cells grown to confluence showed significant cytoplasmic retention of VPs (Fig. 2, right panels), consistent with the impaired capsid assembly and virus maturation under this culture condition (Gil-Ranedo *et al*., 2015). These results demonstrated that: (i) the Nt domains were not accessible to antibodies in the cytoplasm; (ii) the nuclear 1Nt exposure required low cell density in wt, but not in VP1-only transfections; and (iii) the 2Nt was only exposed in the nucleus of productively transfected cells. Therefore, the previously recognized VP2 mediated cell cycle regulation of MVM assembly (Gil-Ranedo *et al*., 2015) involves the masking of the 1Nt and 2Nt domains by the VP2 subunits.

Differential Nt exposures in nuclear MVM capsid assembly intermediates.

To further investigate the nuclear stages of the MVM assembly process, we analyzed the exposure of 1Nt and 2Nt in trimers and larger VP oligomers accumulated in the nucleus prior to viral particles formation. For this, we used the VP-expressing wt (pSVtk-VPs; Sánchez-Martínez *et al*., 2012), and the derivative K153A and L565W mutant plasmids lacking inter-subunits contacts (Reguera *et al.,* 2004), which yielded trimers (8.9 S) and uncharacterized larger (approximate 30 S) nuclear subviral assemblies respectively (Riolobos *et al*, 2006). A preliminary study was required to establish culture conditions supporting cell cycle control of VPs nuclear transport in transiently transfected cells. As shown in Fig. 3A, pSVtk-VPs transfected cells seeded at low density showed efficient

nuclear capsid formation (growing cultures), but culturing at high density led to a significant cycle arrest at G1, marked impairment of VPs nuclear transport, and capsid assembly restricted to a weak punctuated cytoplasmic phenotype (Fig. 3A, density arrest). Under these satisfactory culture conditions, transfections at low cell density (Fig. 3B, left growing panels) displayed uniform (wt-VPs, and K153A) or punctuated (L565W) nuclear VPs staining, as previously reported (Riolobos *et al.,* 2006). The wt and both mutant assemblies clearly exposed the 1Nt domain in the nucleus (Fig. 3B, left panels). At high cell density though the nuclear accumulation of wt and mutant VPs subunits was severely impaired, as above, and the accessibility of their 1Nt domains significantly declined even inside the nucleus, suggesting structural masking (Fig. 3B, right panels). Under this culture condition of inhibited VPs transport, instead of a fine punctuated phenotype, the L565W mutant yielded large cytoplasmic circles and dots reassembling ubiquitin-conjugated aggregates found in some assembly incompetent VP1/ΔVP2 deletion mutants (Lombardo *et al*., 2002). The 2Nt domain was not accessible in any assembly intermediate regardless of the subcellular accumulation, consistent with the absence in these plasmids of nonstructural proteins essential for genome replication and 2Nt exposure in mature virus (Maroto *et al*., 2004) and packaging intermediates (Cotmore and Tattersall, 2005). These experiments: (i) confirmed that the Nt domains are not accessible to antibodies in the cytoplasmic assembly intermediates; (ii) demonstrated that trimers undergo a conformational shift upon nuclear translocation exposing 1Nt in the heterotrimer, but keeping 2Nt hidden in both types of trimers; and (iii) further showed that trimers and larger subviral assembly intermediates accumulated in the nucleus maintain the 1Nt exposed.

Exposure of the 1Nt and 2Nt domains throughout the MVM synchronous infection cycle.

To determine whether the MVM assembly results obtained in transfection studies were supported in the context of natural infection, we analyzed the exposure of the Nt domains along the VPs subcellular distribution and assembly in a synchronous infection cycle (Fig. 4). NB324K cells infected by purified MVM (MOI 5), showed weak signals from the input viral particles while under G1/S aphidicolin arrest (Fig. 4; 0 hpa panels). As cells released from the arrest moved into S phase (Fig. 4A; 6 hpa), the expressed VPs filled the cytoplasm and underwent simultaneous nuclear translocation to a mixed phenotype (Fig. 4B; 6 hpa panels), with weak capsid and 1Nt staining confined to the nucleus in less than 8 % of the cells. When the S /G2 phases boundary was reached and cells showed marked nuclear accumulation of VPs (Fig. 4; 8 hpa panels), a significant increase in the capsid and 1Nt nuclear staining was demonstrated, whereas weak 2Nt nuclear staining became first evident in a low percentage of cells. At late times of the infection cycle, when the bulk of viral genome replication takes place (Gil-Ranedo *et al*., 2015), infected cells showed a patent S/G2 arrest as compared to the predominant G2/G1 phase of uninfected cells (Fig. 4A; 10 hpa), and most nuclei stained intensely with all four antibodies (Fig. 4B; 10 hpa panels). This experiment showed that during infection, as in transfection: (i) the 1Nt and 2Nt domains are not exposed in cytoplasmic protein subunits and assembly intermediates; (ii) the VPs translocation into the nucleus at mid S phase led to 1Nt exposure coinciding with the rise of capsid assembly; (iii) upon VPs nuclear accumulation not only capsid but also 1Nt staining remained positive throughout the final stages of the infection cycle; and (iv) the 2Nt was newly exposed at times of virus genome replication and maturation.

Empty and DNA-filled viral particles drastically differ in the phosphorylation level of their VP1 subunits.

Following the assembly pathway VPs oligomers form the MVM particles in the nucleus (Lombardo *et al*., 2000; Riolobos *et al*., 2006). The MVM empty capsid assembled in NB324K cells had protein subunits modified in a specific 2-D pattern of Ser/Thr phosphorylation (Maroto *et al*., 2000). To investigate a possible role of VPs phosphorylation in MVM maturation, the phosphorylation status of the VP1 and VP2 subunits assembled in *in vivo* ^{32}P-labelled empty capsid and DNA-filled virus highly purified from NB324K cells at 40 hpi (see Materials and Methods) was carefully re-examined. Empty capsids harbored a VP1:VP2 phosphorylation ratio close to their 1:5 stoichiometry of synthesis (Fig. 5). However, this ratio was at least fourfold lower in the DNA-filled virus purified from two independent experiments, as the viral VP1 subunits consistently showed barely detectable phosphorylation (Fig. 5; Exp #1 and #2). To rule out deficient transfer to filters of putative highly phosphorylated VP1 protein species, the actual phosphorylation level of the VPs subunits assembled in both types of viral particles was determined inside the resolving gels. An in gel extensive removal of the abundant phospholabel from the ssDNA genome backbone was required to visualize the virus phosphoproteins (see Materials and Methods). As shown in Fig. 5 (Exp#2; right panel), the autoradiography of gels subjected to this treatment confirmed the virtually unphosphorylated status of the VP1 subunits assembled in the DNA-filled virus.

Pattern of VP2 phosphorylation and dephosphorylation in MVM particles.

Unlike VP1, the VP2 subunits of purified viruses remained significantly phosphorylated (Fig. 5), prompting us to study in greater detail whether viral genome packaging involves alteration of the VP2 phosphorylation pattern. For this, the VP2 protein subunits of ^{32}P-labelled MVM empty capsids and DNA-filled viruses purified as above were subjected to 2D tryptic phosphopeptides analysis. As shown in Fig. 6 (*upper left panel*), the VP2

subunits of empty capsids showed the characteristic 2-D phosphopeptides map previously reported (Maroto *et al*., 2000). Albeit the limited availability of ^{32}P counts in the proteins of highly purified virus samples, the overall 2D phosphopeptides pattern was fairly preserved in the virus VP2 subunits. However, one of the main VP2 capsid phosphopeptides, termed I in the original described map (Maroto *et al.,* 2000), showed a relative phosphorylation level significantly lower in the virus ^{32}P-fingerprints (Fig 6, *lower left panel*). This selective under-representation of phosphopeptide I was consistently observed in three independent virus purifications (data not shown).

Finally, we focused on the phosphorylation status of the virus-specific VP3 subunits, a protein resulting from the 2Nt-cleavage off VP2 protein as the incoming virus traffic through the endosome (Sánchez-Martínez *et al.,* 2012; and references therein). Remarkably, an absolute dephosphorylated stage was observed for the VP3 protein blotted to filters (Fig. 5), as well as for the protein analyzed inside the resolving gels (Fig. 5, *lower right panel*). The lack of phospholabel in VP3 was consistent with the phosphoserine residues that mapped to the 2Nt (Maroto *et al*., 2000), and with the severe dephosphorylation of peptide I in the virus VP2 (Fig. 6). In conclusion, as only the uncleaved virus VP2 subunits maintained most VP2 phosphopeptides, the phosphorylation level of the protein coat in DNA-filled virus is markedly lower than that of the empty capsid.

Discussion

Nuclear icosahedral DNA viruses of animals share the common need to protect their genome during cytoplasmic trafficking until its delivery into the nucleus, and to orchestrate an assembly pathway of asymmetric structural subunits that must translocate across the nuclear envelope to package the genome. However, their strategies, cellular effectors, and molecular mechanisms are widely diverse. The life cycle of the ssDNA viruses of the *Parvoviridae* proceeds through highly efficient concatenated processes that are tightly dependent on cell physiology, which complicates its molecular characterization. We found necessary the use of mutants halting the assembly process at specific stages (Lombardo *et al.,* 2000, 2002; Riolobos *et al.,* 2006), synchronization of infected and transfected cells (Gil-Ranedo *et al.,* 2015), and 2-D high resolution of capsid subunits phosphorylation patterns (Maroto *et al.,* 2000, 2004; Riolobos *et al.,* 2010), to interpret parvovirus MVM assembly data. In this report, these methodologies were used to search additional configuration and phosphorylation features of assembly intermediates and MVM particles. To facilitate understanding, our major findings have been integrated into the model depicted in Fig. 7, which is discussed below.

Role of Nt exposure and phosphorylation in the cell cycle-regulated nuclear transport of parvovirus capsid subunits.

Studying cytoplasmic VPs assembly in transfected cells arrested in G1 by contact inhibition is relevant to what happens in a productive MVM infection, as VPs expression occurs soon after release of the G1/S arrest, several hours prior viral genome replication, and moreover infected cells subjected to cycle arrest at G1 showed significant VPs expression (Gil-Ranedo et al., 2015). The MVM capsid subunits expressed in G1/S

synchronous cells were isolated as cytoplasmic homo- 3VP2, and hetero- 2VP2:1VP1 trimers (Fig. 1), consistent with the composition of these early assembly intermediates obtained by chemical cross-linking and sedimentation (Riolobos *et al*., 2006). In the configuration adopted in the cytoplasm, the Nt domains of the trimeric subunits were not accessible to antibodies in transfected or infected cells (Fig. 2-4), suggesting their structural and functional masking. As 1Nt harbors a consensus NLS, which suffices for the nuclear transport of singly expressed VP1 proteins (Lombardo *et al*., 2002; Vihinen-Ranta *et al*., 2002), its functional inactivation must be accounted for by the cytoplasmic interaction of VP1/VP2 subunits in the heterotrimer. This masking would also explain why 1Nt is incompetent to drive the cell cycle dependent VPs transport (Gil-Ranedo *et al*., 2015, and Fig. 2).

In the restricted conformational and functional cytoplasmic 1Nt exposure, phosphorylation may play a role, as the phosphorylation level of the VP1 subunits in the cytoplasmic heterotrimers was five fold higher than that of the VP2 (Fig. 1B, C). In purified empty capsids, VP1 was phosphorylated at multiple Ser and Thr residues (Maroto *et al*., 2000), but the localization of these residues, and their relationship with the cytoplasmic hyper-phosphorylation of the heterotrimer, remains to be characterized. Inside the nucleus VP1 subunits are subjected to an orchestrated dephosphorylation programme during subsequent steps of the viral life cycle (Fig. 5). Interestingly, after nuclear translocation, heterotrimers displayed an exposed 1Nt (Fig. 3 and 4), a conformation switch that may be coordinated by dephosphorylation and confer directionality to the assembly pathway (Fig. 7).

In contrast, the 2Nt domain was hidden (Fig. 2 to 4), and remained at similar phosphorylation levels (Gil-Ranedo *et al*., 2015), in both cytoplasmic and nuclear trimers. The inaccessibility of 2Nt during during nuclear import may structurally mask its export activity (Maroto *et al.,* 2004). It is also possible that this hidden 2Nt conformation is regulated by phosphorylation, as a Raf-1 kinase mediated phosphorylation, which targeted three serine residues located within 2Nt, was strictly required for VP2 nuclear import (Riolobos et al., 2010). Therefore, the phosphorylation status of the cytoplasmic trimers may impose a configuration in which both 1Nt and 2Nt are hidden and functionally inactive, and inter-trimer contacts blocked to avoid premature capsid assembly. In response to other cellular signals or factors yet to be characterized, trimers with proper folding of the NLM (Lombardo *et al*., 2000) would access a non-conventional transport route, driving VPs into the nucleus via a cell cycle-coupled mechanism (Gil-Ranedo *et al*., 2015).

Capsid subunits configuration and phosphorylation in nuclear assembly and virus maturation.

This study suggests that the parvovirus assembly pathway increases complexity inside the nucleus, as it may be illustrated by the 1Nt exposure. Although the 1Nt is concealed within the coat of purified parvovirus viral particles inaccessible to antibodies or proteases *in vitro* (Cotmore *et al*., 1999; Hernando *et al*., 2000; Maroto *et al*., 2004; Mani *et al*., 2006; Popa-Wagner *et al*., 2012; Venkatakrishnan *et al*., 2013), an important 1Nt exposure was observed in the nuclei of infected and transfected cells expressing trimers and larger assembly intermediates (Fig. 2 to 4). Interestingly, nuclear 1Nt nuclear staining was particularly intense at late times of the synchronous infection (Fig. 4). In the absence of evidences for procapsids or characterized large subviral assemblies bearing exposed 1Nt, the significance of the maintained nuclear 1Nt staining remains uncertain.

During MVM maturation, the DNA-filled virus lacked all the VP1 phosphorylation sites (Fig. 5) and one major VP2 phosphopeptide (Fig. 6) found in the empty capsid. This disparate phosphorylation status between the two major nuclear viral particles may suggest a role of phosphates in viral genome packaging. The most widely accepted model delineates parvovirus maturation via an helicase-mediated pumping of the ssDNA genome into preformed capsids through a fivefold pore (King *et al.,* 2001; Cotmore and Tattersall, 2005; Plevka *et al.,* 2011). Fitting our data with this model might suggest that the packaging machinery select for a subpopulation of empty capsids harboring dephosphorylated VP1 subunits, or that drastic VPs dephosphorylation accompanies viral genome encapsidation. The removal of phosphate substituents from VP1 subunits, and a precise VP2 phosphorylation status with 2Nt exposure, may be required for specific packaging of the parvovirus negatively charged ssDNA genome. Further research addressing the phosphorylation of large VPs complexes and viral particles, and their viral ssDNA specific interactions, will be required to understand the complex nuclear events regulating parvovirus assembly and maturation.

Phosphates and Nt domains in viral trafficking.

The routing signals mapped in 1Nt and 2Nt led us to propose that the mature MVM would alternatively expose these flexible domains for trafficking (Maroto *et al*., 2004), a concept subsequently extended to other parvoviruses (Popa-Wagner *et al*., 2012; Boisvert *et al*., 2014). Consistently with this view, VP2-Nt became exposed only at late times of the infection cycle (Fig. 4), suggesting that its function is restricted to the traffic of mature virus. The exposure and phosphorylation of 2Nt may thus be relevant to both viral import and export. Indeed, 2Nt plays, as 1Nt, an essential role for the MVM infectious entry pathway (see Introduction). In virus particles purified from transformed NB324K cells, 2Nt

was heavily phosphorylated (Maroto *et al*., 2000), but during cell entry most terminal domains are cleaved-off VP2 in the endosome (Sánchez-Martínez *et al*., 2012, and references therein), and this study shows that the resulting VP3 subunits are, as with VP1, virtually unphosphorylated (Fig. 5). This result raises issue about the actual phosphorylation status of the remaining VP2 subunits in post-endosomal incoming virus particles. Although the VP2 of total virus lacked, in respect to empty capsid, only the phosphorylation site(s) of phosphopeptide I (Fig. 6), we did not compare the phosphorylation status of VP2 in virus purified from the medium and different cellular compartments. Regardless of this uncertainty about VP2, the post-endosomal viral particles routing to the nucleus have a very low or completely dephosphorylated status, a chemical feature that may be required for successful nuclear genome delivery.

The role that capsid phosphorylation plays in parvovirus egress from the nucleus, and from other cellular compartments, is less understood. In NB324K cells, the 2Nt of the MVMp strain was phosphorylated by cytoplasmic Raf-1 kinase (Riolobos *et al*., 2010), and this modification greatly facilitated viral nuclear egress (Maroto *et al*., 2004). However, in A9 mouse fibroblasts expressing low Raf-1 activity (Riolobos *et al*., 2010), MVMp nuclear egress operated by an NS2-CRM1 mediated export pathway (Eichwald *et al*., 2002; Miller and Pintel, 2002; Engelsma *et al*., 2008), which paradoxically benefited from mutations inactivating the 2Nt serine phosphorylation sites (Maroto et al., 2004). It was recently reported that lambda phosphatase-sensitive negative charges exposed on the MVMp capsid surface at sites unrelated to 2Nt phosphoserines were enriched in virus particles with nuclear export potential in A9 cells (Wolfisberg *et al.,* 2016). Although further research on the nature and protein distribution of these charges is required to correlate them with NS2

functions and our phosphorylation studies, the overall data are consistent with a 2Nt phosphorylation-independent nuclear export route in A9 cells. Interestingly, when challenging the MVMi strain by a passive neutralizing polyclonal therapy in mice, viruses that emerged after evading the immune pressure carried mutations located exclusively within the NS2-CRM1 binding domain, and these mutations increased NS2-CRM1 binding affinity and enhanced MVMi egress in NB324K cells (Lopez-Bueno *et al.,* 2004). Therefore, the available information from different experimental systems supports that the NS2- and 2Nt- mediated routes of viral nuclear export are mechanistically linked in a cell type-dependent manner. This connection may regulate virus spread and fitness in tissues.

Conclusions

This study shows that specific phosphorylations and changes in the conformation of the N-terminal domains of capsid subunits may contribute to the fine-tuned cell cycle coupling of parvovirus assembly, genome encapsidation, and viral trafficking. While cytoplasmic trimers and their transport regulation could be characterized, inside the nucleus the assembly pathway involved differential phosphorylation and configuration of multiple assembly intermediates and viral particles, a complexity challenging our understanding of the maturation process of these small viruses. Our study may provide important implications for the assembly of other nuclear icosahedral viruses, in particular those encoding protein subunits undergoing post-translational phosphorylation. It also points toward a network of cell cycle regulatory signals and factors that acting at the level of protein phosphorylation may become potential targets for wide antiviral interventions.

Acknowledgments

JG-R, EH, and NV equally contributed to this work. We thank P. Tattersall (Yale, CT) for providing the pMVM infectious plasmid and the VP1-specific polyclonal antibody. This article is in the memory of Juan Fernandez Santarén and his unique legacy of 2-D resolved proteins.

Funding Information

This work was supported by the grants SAF2011-29403 (Spanish Ministerio de Ciencia e Innovación), SAF2015-68522-P-MINECO/FEDER, UE (Spanish Ministerio de Economía y Competitividad), and S2013/ABI-2906-FEDER (Comunidad de Madrid), to JMA, and by institutional grants from the Fundación Ramón Areces and Banco Santander to the Centro de Biología Molecular Severo Ochoa (CSIC-UAM).

References

Agbandje-McKenna, M., A. L. Llamas-Saiz, F. Wang, P. Tattersall, and M. G. Rossmann. 1998. Functional implications of the structure of the murine parvovirus, minute virus of mice. Structure 6:1369–1381.

Bjorn-Patrick, M., and P. Roy. 2016. Cellular casein kinase 2 and protein phosphatase 2A modulate replication site assembly of bluetongue virus. J. Biol. Chem. 291: 14566-14574.

Boisvert, M., Bouchard-Lévesque, V., Fernandes, S., and P. Tijssen. 2014. Classic nuclear localization signals and a novel nuclear localization motif are required for nuclear transport of porcine parvovirus. J. Virol. 88: 11748-11759.

Boisvert, M., Fernandes, S., and P. Tijssen. 2010. Multiple pathways involved in porcine parvovirus cellular entry and trafficking toward the nucleus. J. Virol. 84: 7782-92.

Brownstein, D. G., A. L. Smith, R. O. Jacoby, E. A. Johnson, G. Hansen, and P. Tattersall. 1991. Pathogenesis of infection with a virulent allotropic variant of minute virus of mice and regulation by host genotype. Lab. Invest. 65:357–363.

Carreira, A., Menendez, M., Reguera, J., Almendral, J.M. and M. G. Mateu. 2004. In vitro disassembly of a parvovirus capsid and effect on capsid stability of heterologous peptide insertions in surface loops. J. Biol. Chem. 279: 6517-6525.

Castellanos, M., Pérez, R., Rodríguez-Huete, A., Grueso, E., Almendral, J.M, and M. G. Mateu. 2013. A slender tract of glycines is required for translocation of protein VP2 N-terminal domain through the parvovirus MVM capsid channel to initiate infection. Biochem. Journal 455: 87-94.

Cotmore, S., Agbandje-McKenna, M., Chiorini, J.A., Mukha, D.V., Pintel, D.J., Qiu, J.M., Soderlund-Venermo, M., Tattersall, P., Tijssen, P., Gatherer, D., and A. J. Davisonet. 2014. The family Parvoviridae. Arch Virol. 159:1239-1247.

Cotmore, S.F., D´Abramo. A.M. Jr., Ticknor, C.M., and P. Tattersall. 1999. Controlled conformational transitions in the MVM virion expose the VP1 N-terminus and viral genome without particle disassembly. Virology 254: 169-181.

Cotmore, S.F., and P. Tattersall. 2005. Encapsidation of minute virus of mice DNA: aspects of the translocation mechanism revealed by the structure of partially packaged genomes. Virology 336: 100–112.

Cotmore, S.F., and P. Tattersall. 2007. Parvoviral host range and cell entry mechanisms. Adv. Virus Res. 70: 183-232.

Cotmore, S.F., and P. Tattersall. 2014. Parvoviruses: small does not mean simple. Annu. Rev. Virol. 1: 517-537.

Crawford, L. V. 1966. A minute virus of mice. Virology 29:605-612.

Eichwald V, Daeffler L, Klein M, Rommelaere J, and N. Salomé. 2002. The NS2 proteins of parvovirus minute virus of mice are required for efficient nuclear egress of progeny virions in mouse cells. J. Virol. 76:10307–10319.

Engelsma, D., Valle, N., Fish, A., Salomé, N., Almendral, J.M., and M. Fornerod. 2008. A supraphysiological nuclear export signal is required for parvovirus nuclear export. Mol. Biol. Cell 19: 2544–2552.

Farr, G.A., Cotmore, S.F., and P. Tattersall. 2006. VP2 cleavage and the leucine ring at the base of the fivefold cylinder control pH-dependent externalization of both the VP1 N terminus and the genome of minute virus of mice. J. Virol. 80: 161–171.

Farr, G.A., Zhang, L., and P. Tattersall. 2005. Parvoviral virions deploy a capsid-tethered lipolytic enzyme to breach the endosomal membrane during cell entry. Proc. Natl. Acad. Sci. USA 102: 17148-17153.

Gardiner E.M., and P. Tattersall. 1988. Mapping of the fibrotropic and lymphotropic host range determinants of the parvovirus minute virus of mice. J. Virol. 62: 2605–2613.

Gil-Ranedo, J., Hernando, E., Riolobos, L., Dominguez, C., Kann, M., and Almendral, J.M. 2015. The mammalian cell cycle regulates parvovirus nuclear capsid assembly. PloS Pathogens. 11(6):e1004920.

Gurda, B. L., Parent, K. N., Bladek, H., Sinkovits, R. S., DiMattia, M. A., Rence, C., Castro, A., McKenna, R., Olson, N., Brown, K., Baker, T. S., and M. Agbandje-McKenna. 2010. Human bocavirus capsid structure: insights into the structural repertoire of the parvoviridae. J. Virol. 84: 5880-9.

Hernando, E., Llamas-Saiz, A.L., Foces-Foces, C., McKenna, R., Portman, I., Agbandje- McKenna, M., and J.M. Almendral. 2000. Biochemical and physical characterization of parvovirus minute virus of mice virus-like particles. Virology 267: 299–309.

Hoque, M., K.-I. Ishizu, A. Matsumoto, S.-I. Han, F. Arisaka, M. Takayama, K. Suzuki, K. Kato, T. Kanda, H. Watanabe, and H. Handa. 1999. Nuclear transport of the major capsid protein is essential for adeno-associated virus capsid formation. J. Virol. 73:7912-7915.

Johnson, J. S., Li, C., DiPrimio, N., Weinberg, M. S., McCown, T. J., and R. J. Samulski. 2010. Mutagenesis of adeno-associated virus type 2 capsid protein VP1 uncovers new roles for basic amino acids in trafficking and cell-specific transduction. J. Virol. 84: 8888-902.

Kaufmann, B., Chipman, P. R., Kostyuchenko, V. A., Modrow, S., and M.G. Rossmann. 2008. Visualization of the externalized VP2 N termini of infectious human parvovirus B19. J. Virol. 82: 7306-12.

Kaufmann B., Lopez-Bueno A., Mateu M.G., Chipman P.R., Nelson C.D., Parrish, C.R., Almendral, J.M., and M. G. Rossmann. 2007. Minute virus of mice, a parvovirus, in complex with the Fab fragment of a neutralizing monoclonal antibody. J. Virol. 81: 9851-9858.

Kaufmann, B., Simpson, A. A., and M.G. Rossmann. 2004. The structure of human parvovirus B19. Proc. Natl. Acad. Sci. U S A. 101: 11628-33.

King J.A., Dubielzig R., Grimm S.W., and J.A. Kleinschmidt. 2001. DNA helicase-mediated packaging of adeno-associated virus type 2 genomes into preformed capsids. EMBO J. 20: 3282–3291.

Kontou, M., L. Govindasamy, H.-J. Nam, N. Bryant, A. L. Llamas-Saiz, C. Foces-Foces, E. Hernando, M.-P. Rubio, R. McKenna, J. M. Almendral, and M. Agbandje-McKenna. 2005. Structural determinants of tissue tropism and *in vivo* pathogenicity for the parvovirus minute virus of mice. J. Virol, 79:10931-10943.

Mani, B., Baltzer, C., Valle, N., Almendral, J. M., Kempf, C., and C. Ros. 2006. Low pH-dependent endosomal processing of the incoming parvovirus minute virus of mice virion leads to externalization of the VP1 N-terminal sequence (N-VP1), N-VP2 cleavage, and uncoating of the full-length genome. J. Virol. 80: 1015-24.

Lombardo, E., J.C., Ramírez, M. Agbandje-Mckenna, and J.M. Almendral. 2000. A ß-stranded motif drives capsid proteins oligomers of the parvovirus minute virus of mice into the nucleus for viral assembly. J. Virol. 74:3804-3814.

Lombardo, E., Ramírez, J.C., García, J., and J.M. Almendral. 2002. Complementary roles of multiple nuclear targeting signals in the capsid proteins of the parvovirus minute virus of mice during assembly and onset of infection. J. Virol. 76: 7049-7059.

Lopez-Bueno A., Mateu M.G., and J. M. Almendral. 2003. High mutant frequency in populations of a DNA virus allows evasion from antibody therapy in an immunodeficient host. J. Virol. 77: 2701-2708.

Lopez-Bueno, A., Valle, N., Gallego, J.M., Perez, J. and J.M. Almendral. 2004. Enhanced cytoplasmic sequestration of the nuclear export receptor CRM1 by NS2 mutations developed in the host regulates parvovirus fitness. J. Virol. 78: 10674-10684.

Manning, G., Whyte, D. B., Martinez, R., Hunter, T., and S. Sudarsanam. 2002. The protein kinase complement of the human genome. Science 298: 1912–1934.

Maroto, B., Ramírez, J.C., and J.M. Almendral. 2000. Phosphorylation status of the parvovirus minute virus of mice particle: mapping and biological relevance of the major phosphorylation sites. J. Virol. 74: 10892-10902.

Maroto, B., N. Valle, R. Saffrich, and J.M. Almendral. 2004. Nuclear export of the non-envelopped parvovirus virion is directed by an unordered protein signal exposed on the capsid surface. J. Virol. 78: 10685-10694.

Miller, C.L., and D.J. Pintel. 2002. Interaction between parvovirus NS2 protein and nuclear export factor Crm1 is important for viral egress from the nucleus of murine cells. J. Virol 76: 3257–3266.

Mondal, A., Potts, G.K., Dawson, A.R., Coon, J.J., and A. Mehle. 2015. Phosphorylation at the homotypic interface regulates nucleoprotein oligomerization and assembly of the influenza virus replication machinery. PLoS Pathogens 11(4):e1004826.

Naumer, M., Sonntag, F., Schmidt, K., Nieto, K., Panke, C., Davey, N.E., Popa-Wagner, R., and J. A. Kleinschmid. 2012. Properties of the AAV assembly activating protein AAP. J. Virol. 86: 13038-13048.

Parrish, C.P. 2010. Structures and functions of parvovirus capsids and the process of cell infection. Curr. Top. Microbiol. Immunol. 343: 149-176.

Pillet, S., Annan, Z., Fichelson, S., and F. Morinet. 2003. Identification of a nonconventional motif necessary for the nuclear import of the human parvovirus B19 major capsid protein (VP2). Virology 306, 25-32.

Plevka P., Hafenstein S., Li L., D'Abramo A., Cotmore S.F., Rossmann M.G., and P. Tattersall. 2011. Structure of a packaging-defective mutant of minute virus of mice indicates that the genome is packaged via a pore at a 5-fold axis. J. Virol. 85: 4822-4827.

Popa-Wagner, R., M. Porwal, M. Kann, M. Reuss, Marc Weimer, L. Florin, and J. A. Kleinschmidt. 2012. Impact of VP1-specific protein sequence motifs on Adeno-Associated Virus type 2 intracellular trafficking and nuclear entry. J. Virol 86: 9163.

Porwal, M., Cohen, S., Snoussi, K., Popa-Wagner, R., Anderson, F., Dugot-Senant, N., Wodrich, H., Dinsart, C., Kleinschmidt, J.A., Panté, N., and M. Kann. 2013. Parvoviruses cause nuclear envelope breakdown by activating key enzymes of mitosis. PLoS Pathog 9: e1003671.

Ramirez, J. C., Santaren, J. F., and J.M. Almendral. 1995. Transcriptional inhibition of the parvovirus minute virus of mice by constitutive expression of an antisense RNA targeted against the NS-1 transactivator protein. Virology 206: 57-68.

Ramírez, J.C., Fairén, A. and Almendral, J.M. 1996. Parvovirus Minute Virus of Mice strain i multiplication and pathogenesis in the newborn mouse brain are restricted to proliferative areas and to migratory cerebellar young neurons. J. Virol. 70, 8109-8116.

Reguera, J., A. Carreira, L. Riolobos, J. M. Almendral, and M. G. Mateu. 2004. Role of interfacial amino acid residues in assembly, stability, and conformation of a spherical virus capsid. Proc. Natl. Acad. Sci. USA. 101: 2724-2729.

Riolobos, L., Reguera, J., Mateu, M.G., and J.M. Almendral. 2006. Nuclear transport of trimeric assembly intermediates exerts a morphogenetic control on the icosahedral parvovirus capsid. J. Mol. Biol. 357: 1026-1038.

Riolobos, L., Valle, N., Hernando, E., Maroto, B., Kann, M., and J.M. Almendral. 2010. Viral oncolysis that targets Raf-1 signaling control of nuclear transport. J. Virol 84: 2090-2099.

Ros C., N., Bayat, R., Wolfisberg, and J. M. Almendral. 2017. Cell entry of protoparvoviruses. Viruses, 9, 313; doi:10.3390/v9110313

Rubio M.P., Lopez-Bueno, A., and J.M. Almendral. 2005. Virulent variants emerging in mice infected with the apathogenic prototype strain of the parvovirus minute virus of mice exhibit a capsid with low avidity for a primary receptor. J. Virol. 79: 11280–11290.

Sánchez-Martínez, C., Grueso, E., Carroll, M., Rommelaere, J., and J. M. Almendral. 2012. Essential role of the unordered VP2 n-terminal domain of the parvovirus MVM capsid in nuclear assembly and endosomal enlargement of the virion fivefold channel for cell entry. Virology 432: 45-56.

Santarén, J. F., J. C. Ramírez, and J. M. Almendral. 1993. Protein species of the parvovirus Minute Virus of Mice strain MVMp: involvement of phosphorylated VP-2 subtypes in viral morphogenesis. J.Virol. 67: 5126-5138.

Segovia, J.C., Gallego, J.M., Bueren, J.A., and Almendral, J.M. 1999. Severe leukopenia and dysregulated erythropoiesis in SCID mice persistently infected with the Parvovirus Minute Virus of Mice. J Virol., 73, 1774-1784.

Sonntag, F., Bleker, S., Leuchs, B., Fischer, R., and J. A. Kleinschmidt. 2006. Adeno-associated virus type 2 capsids with externalized VP1/VP2 trafficking domains are generated prior to passage through the cytoplasm and are maintained until uncoating occurs in the nucleus. J. Virol. 80: 11040-54.

Sonntag, F., Schmidt, K., and J. A. Kleinschmidt. 2010. A viral assembly factor promotes AAV2 capsid formation in the nucleolus. Proc. Natl. Acad. Sci. USA 107: 10220-10225.

Subramaniana, S., Organtini, L.J., Grossman, A., Domeier, P.P., Cifuente, J.O., Makhov, A.M., Conway, J.F., D'Abramo, A., Cotmore, S.F., Tattersall, P., and S. Hafenstein. 2017. Cryo-EM maps reveal five-fold channel structures and their modification by gatekeeper mutations in the parvovirus minute virus of mice (MVM) capsid. Virology 510 (2017) 216–223

Sugai, A., Sato, H., Hagiwara, K., Kozuka-Hata, H., Oyama, M., Yoneda, M., and C. Kai. 2014. Newly identified minor phosphorylation site threonine-279 of measles virus nucleoprotein is a prerequisite for nucleocapsid formation. J. Virol. 88: 1140-1149.

Tattersall, P., and J. Bratton. 1983. Reciprocal productive and restrictive virus-cell interaction of immunosuppressive and prototype strains of minute virus of mice. J. Virol. 46: 944-955.

Tsao, J., Chapman, M. S., Agbandje, M., Séller, W., Smith, K., Wu, H., Luo, M., Smith, T. J., Rossmann, M. G., Compans, R. W. and C.R. Parrish. 1991. The three-dimensional structure of canine parvovirus and its functional implications. Science 251: 1456-1464.

Tullis, G. E., Burger, L. R., and D. J. Pintel. 1992. The trypsin-sensitive RVER domain in the capsid proteins of minute virus of mice is required for efficient cell binding and viral infection but not for proteolytic processing in vivo. Virology 191: 846-57.

Tullis, G.E., R.B. Lisa, and D. J. Pintel. 1993. The minor capsid protein VP1 of the autonomous parvovirus minute virus of mice is dispensable for encapsidation of progeny single-stranded DNA but is required for infectivity. J. Virol. 67:131-141.

Ubersax, J. A., and J. E. Jr. Ferrell. 2007. Mechanisms of specificity in protein phosphorylation. Nat. Rev. Mol. Cell Biol. 8: 530–541.

Valle, N., Riolobos, R., and J. M. Almendral. 2006. Synthesis, post-translational modification and trafficking of the parvovirus structural polypeptides. In Parvoviruses (Kerr, J.R., Cotmore, S.F., Bloom, M.E., Linden R.M., and Parrish, C.R., eds), pp. 291-304. Edward Arnold, London.

Venkatakrishnan, B., Yarbrough, J., Domsic, J., Bennett, A., Bothner, B., Kozyreva, O.G., Samulski, R.J., Muzyczka, N., McKenna, R., and M. Agbandje-McKenna. 2013. Structure and dynamics of adeno-associated virus serotype 1 VP1-unique n-terminal domain and its role in capsid trafficking. J. Virol. 87:4974-4984.

Vihinen-Ranta, M., D. Wang, W. S. Weichert, and C. R. Parrish. 2002. The VP1 N-terminal sequence of canine parvovirus affects nuclear transport of capsids and efficient cell infection. J. Virol. 76: 1884-1891.

Wolfisberg, R., Kempf, C., and C. Ros. 2016. Late maturation steps preceding selective nuclear export and egress of progeny parvovirus. J. Virol. 90: 5462-5474.

Xie, Q., Bu. W., Bhatia, S., Hare, J., Somasundaram, T., Azzi, A. and M.S. Chapman. 2002. The atomic structure of adeno-associated virus (AAV-2), a vector for human gene therapy. Proc. Nat. Acad. Sci. U S A. 99: 10405-10410.

Yuan, W., and C.R. Parrish. 2001. Canine parvovirus capsid assembly and differences in mammalian and insect cells. Virology 279: 546–557.

Zadori, Z., Szelei, J., Lacoste, M.C., Gariepy, S., Raymond, P., Allaire, M., Nabi, I.R., and P. Tijssen. 2001. A viral phospholipase A2 is required for parvovirus infectivity. Dev. Cell 1: 291-302.

Zhang, K., Brownlie, R., Snider, M., and S. van Drunen Littel-van den Hurk. 2016. Phosphorylation of bovine herpesvirus 1 VP8 plays a role in viral DNA encapsidation and is essential for its cytoplasmic localization and optimal virion incorporation. J. Virol. 90: 4427-4440.

Legends to figures

Fig. 1. Phosphorylation status of capsid subunits in the cytoplasmic MVM assembly intermediates. (**A**) Confocal microscopy of VP subcellular distribution and nuclear capsid formation in VP-expressing NB324K cells growing asynchronously (left), synchronized at G1/S with aphidicolin (middle), and traversing S phase at 8 h post-release of the cell cycle arrest (right). Cellular DNA content determined by flow cytometry (DAPI staining) is shown to the left. CC, cell count. Scale bar, 25 μm. (**B**) Relative phosphorylation of the capsid proteins in G1/S arrested cells. Shown are ^{35}S- or ^{32}P-labeled VP proteins immunoprecipitated from supramolecular assemblies under native (n) or denaturing (d) conditions with the indicated antibodies. Gels were exposed to autoradiography for 48 h, using an intensifying screen at –70 ^{0}C for the ^{32}P-labeled samples. (**C**) Ratio of radiolabeled VP1/VP2 proteins in VP1-containing oligomers (α-VP1, native conditions) or total expressed subunits (α-VPs, denaturing conditions) quantified by densitometry of the films. Bars are means with standard errors from three independent experiments.

Fig. 2. Changes of VPs-Nt configuration during MVM assembly. IF analysis of NB324K cells transfected with the indicated pMVM-derived plasmids and maintained in asynchronous growth (*left*), or subjected to density arrest (*right*). Shown are representative confocal images of VPs subcellular distribution, and of the exposure of N-terminal domains of VP1 (1Nt) and VP2 (2Nt), as stained with specific antibodies. Bars represent average values with errors from three experiments. NA, not applicable.

Fig. 3. Nt configuration in subviral nuclear assemblies. (**A**) Cells transfected with the

pSVtk-VPs plasmid cultured at low density (Growing; seeding at $8x10^3$ cells/cm^2) or to confluence (Density arrest; seeding at $8x10^4$ cells/cm^2) for 48h. *Left*: Flow cytometry analysis of the percentage of transfected cells (VPs^+) allowing capsid formation ($Capsid^+$, Mab-B7 staining). CC, cell count. *Right*: Subcellular distribution of VPs and assembly of capsid proteins in cultures seeded at low density and confluence analyzed by confocal microscopy. (**B**) Cells tranfected with the indicated wt and single mutant VPs-expressing plasmids cultured and analyzed as in Fig. 2. The figure shows representative confocal fields of cells from three experiments. Average values with standard errors from three experiments are shown.

Fig. 4. Exposure of the Nt domains during the MVM synchronous infection cycle. (**A**) Flow-cytometry analysis of DNA content (DAPI staining), VP1-Nt exposure, and capsid formation in synchronously infected NB324K cells. (**B**) Subcellular distribution, capsid assembly, and access to specific antibodies recognizing the Nt domains of viral structural proteins. Scale bars, 25 μm. Shown are representative phenotypes at the indicated hours post-release of isoleucine/aphidicolin arrest (hpa). Bars illustrate the average values with standard errors from four experiments.

Fig. 5. Phosphorylation status of the protein subunits assembled in MVM particles. Relative VPs phosphorylation harbored by *in vivo* ^{32}P-labeled empty capsid (C), and DNA-filled virus (V) purified from two independent experiments. Proteins were resolved by 8%SDS-PAGE and either blotted to filters or fixed in the gels. *Exp.#1*: filters exposed to autoradiography at -70 ^{0}C with intensifying screen (left panel), and subsequently probed

with the α-VPs antibody (right panel). *Exp.#2*: VPs blotted to filters (left panel) or fixed inside the gels (right panel) prior exposure to autoradiography. Below: Ratio of VP1/VP2 signals quantified by densitometry. a.u., arbitrary units.

Fig. 6. VP2 phosphopeptides composition of MVM particles**.** *Left*: Two-dimensional tryptic phosphopeptide maps of the VP2 subunits isolated from *in vivo* ^{32}P-labeled purified empty and DNA-filled viral particles. TLC plates were exposed for 10 days to a radio-analytic imaging system. Main phosphopeptides were designed as previously reported (Maroto et al., 2000). 1D, first dimension; 2D, second dimension. *Right*: Bars represent the signal in the films of the five major VP2 phophopeptides quantified by densitometry from a representative experiment. a.u., arbitrary units.

Fig. 7. Phosphorylation and Nt-configuration of capsid proteins throughout the MVM life cycle. The diagram illustrates phosphorylation levels and exposure of Nt-domains of the VP1, VP2 and VP3 structural proteins (respective numbers in this figure) in the supra-molecular complexes traversing the cytoplasmic and nuclear membranes during the MVM infection cycle. The G_1, S, and G_2 letters (connected by arrows above in the figure) refer to the cell cycle steps at which virus assembly and maturation preferably occur. VP subunits in the viral particles and assembly intermediates are depicted at their estimated stoichiometry. The VP1-Nt and VP2-Nt domains are only illustrated in exposed configuration(s) accessible to antibodies. R: Virus receptor; NPC: Nuclear pore complex.

Figure
Click here to download high resolution image

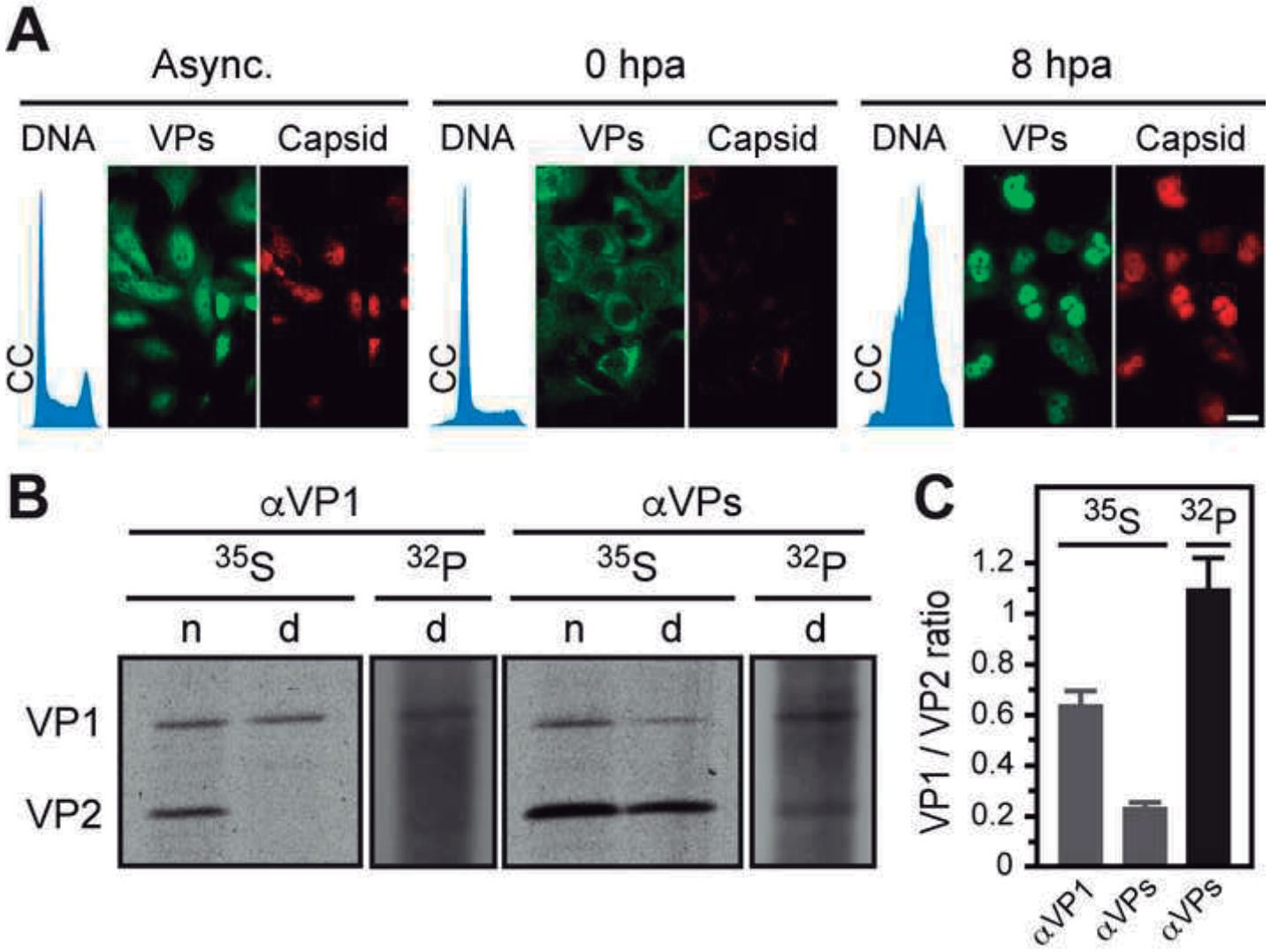

Figure 2
Click here to download high resolution image

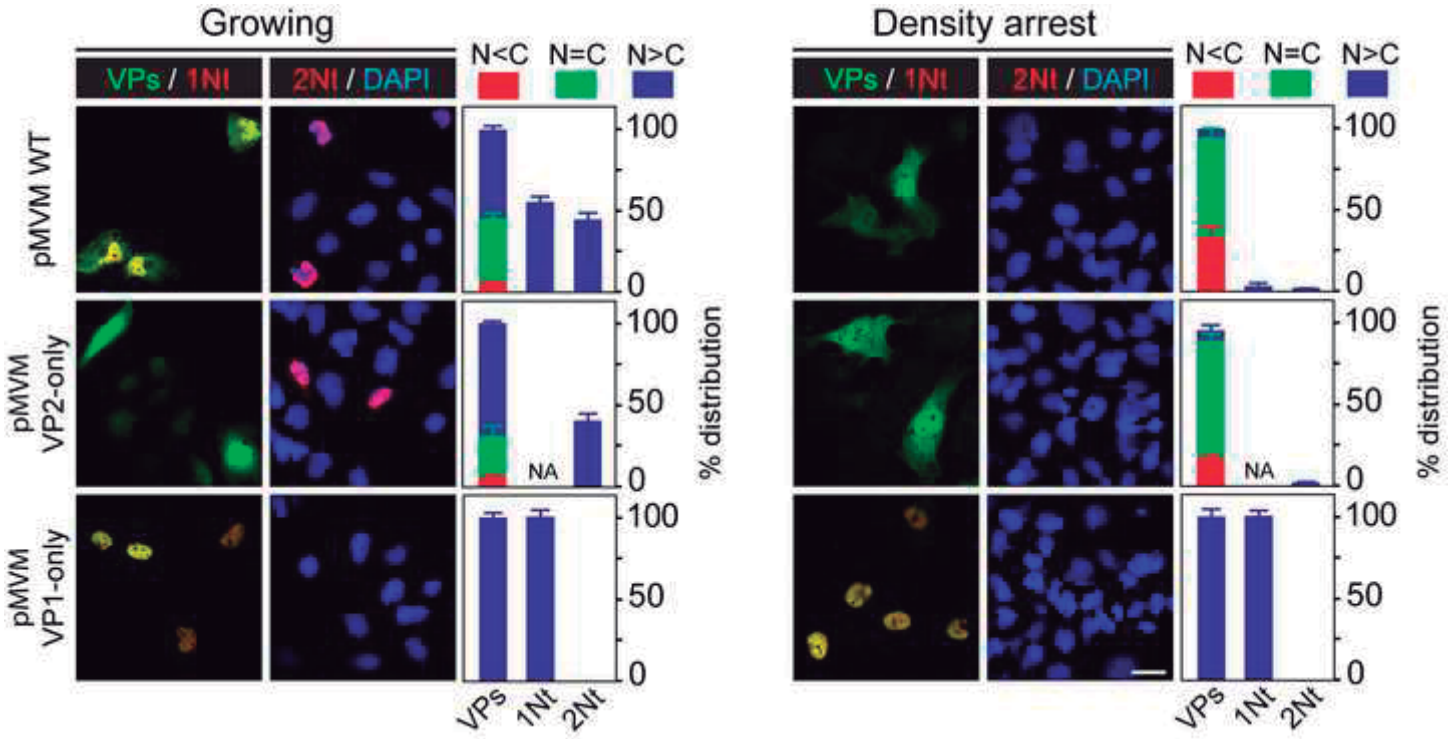

Figure 3
Click here to download high resolution image

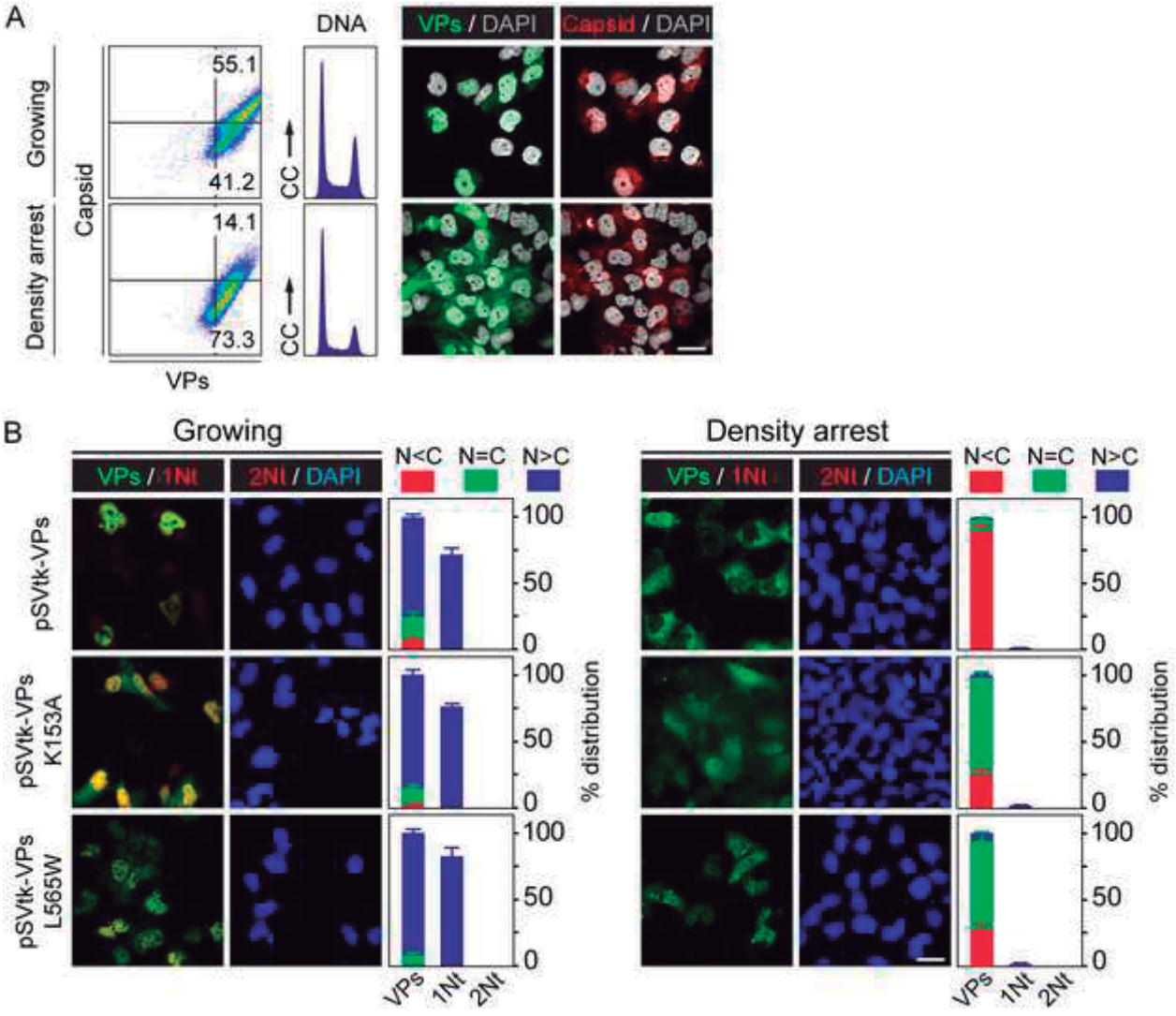

Figure 4
Click here to download high resolution image

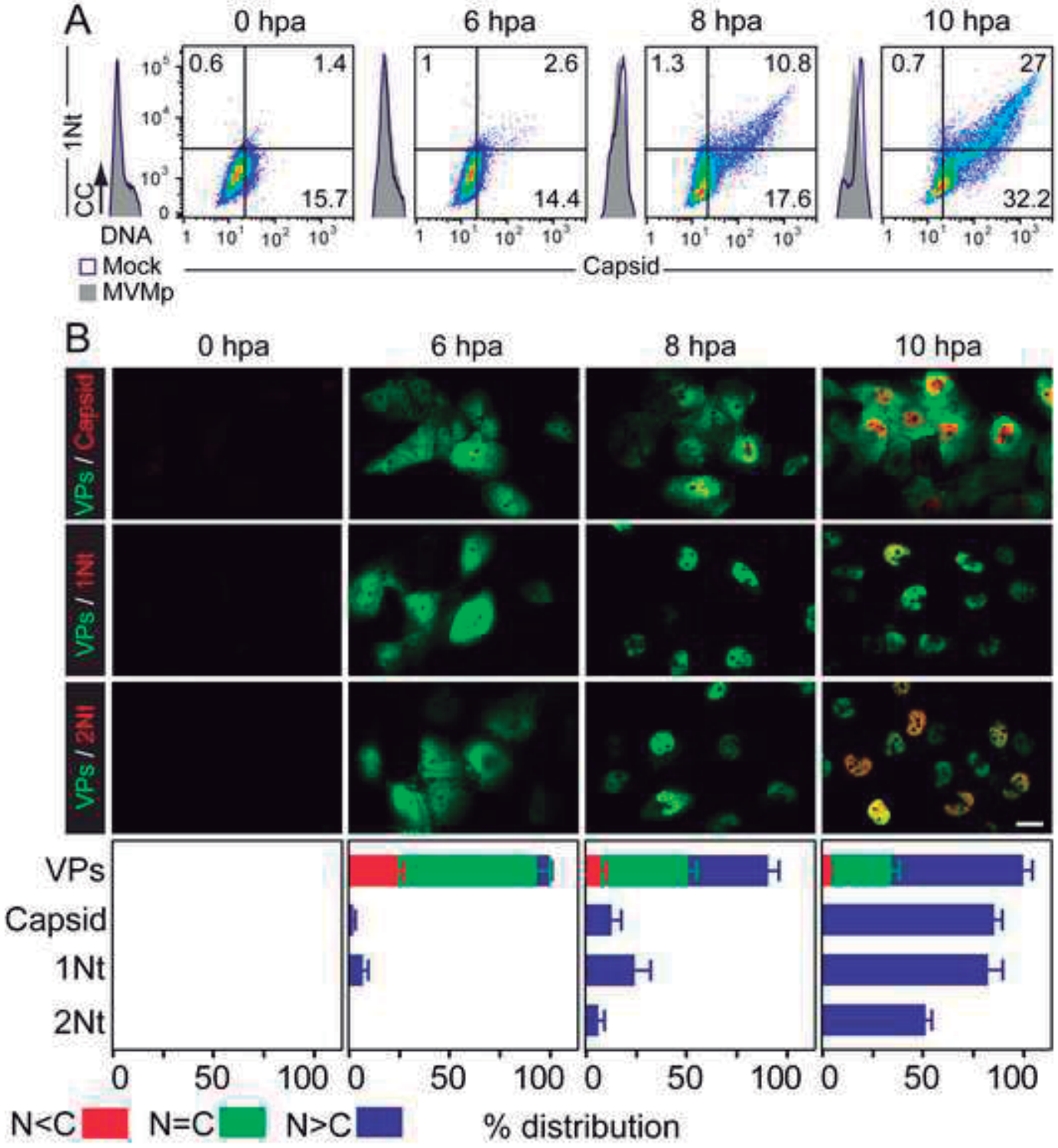

Figure 5
Click here to download high resolution image

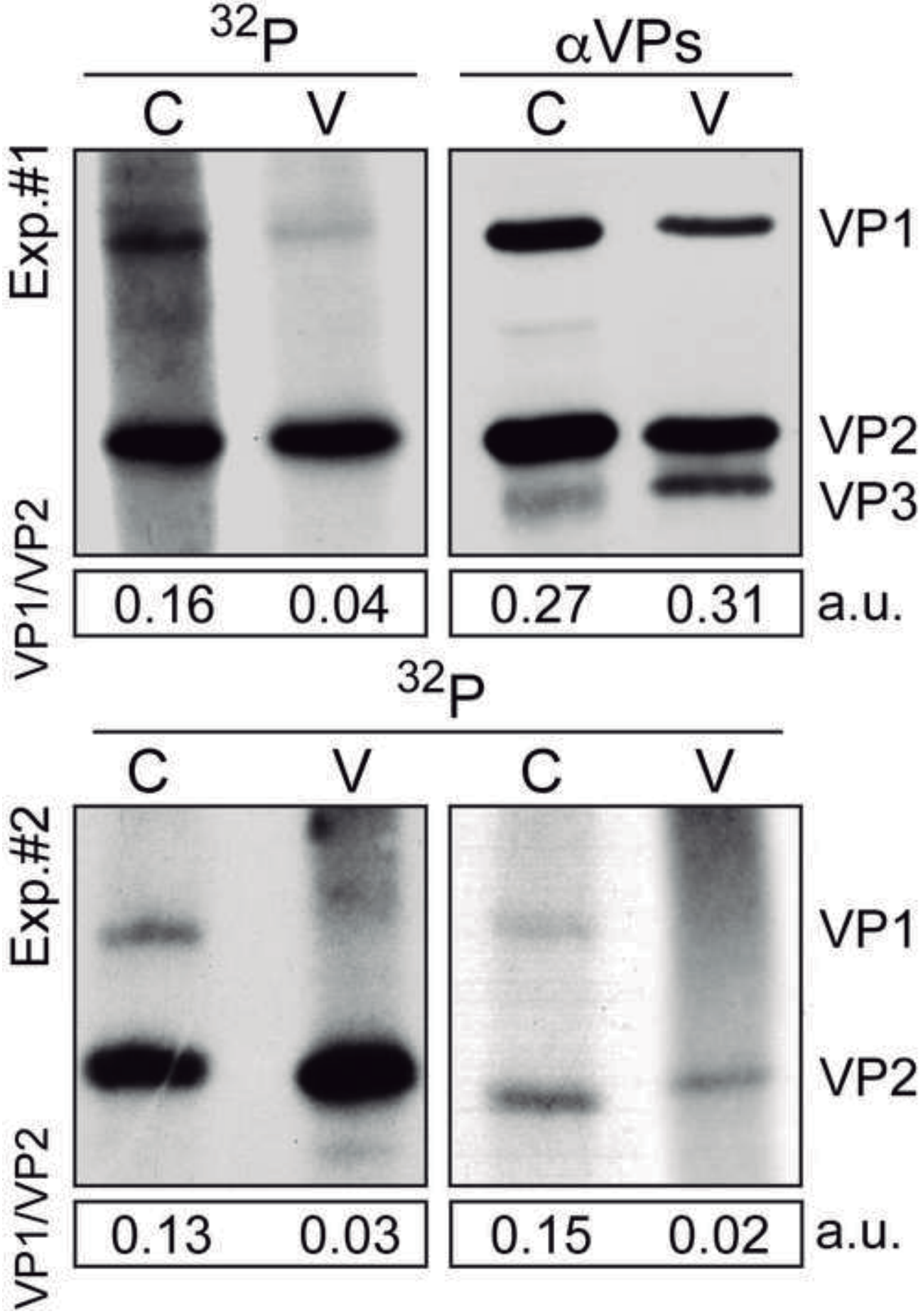

Figure 6
Click here to download high resolution image

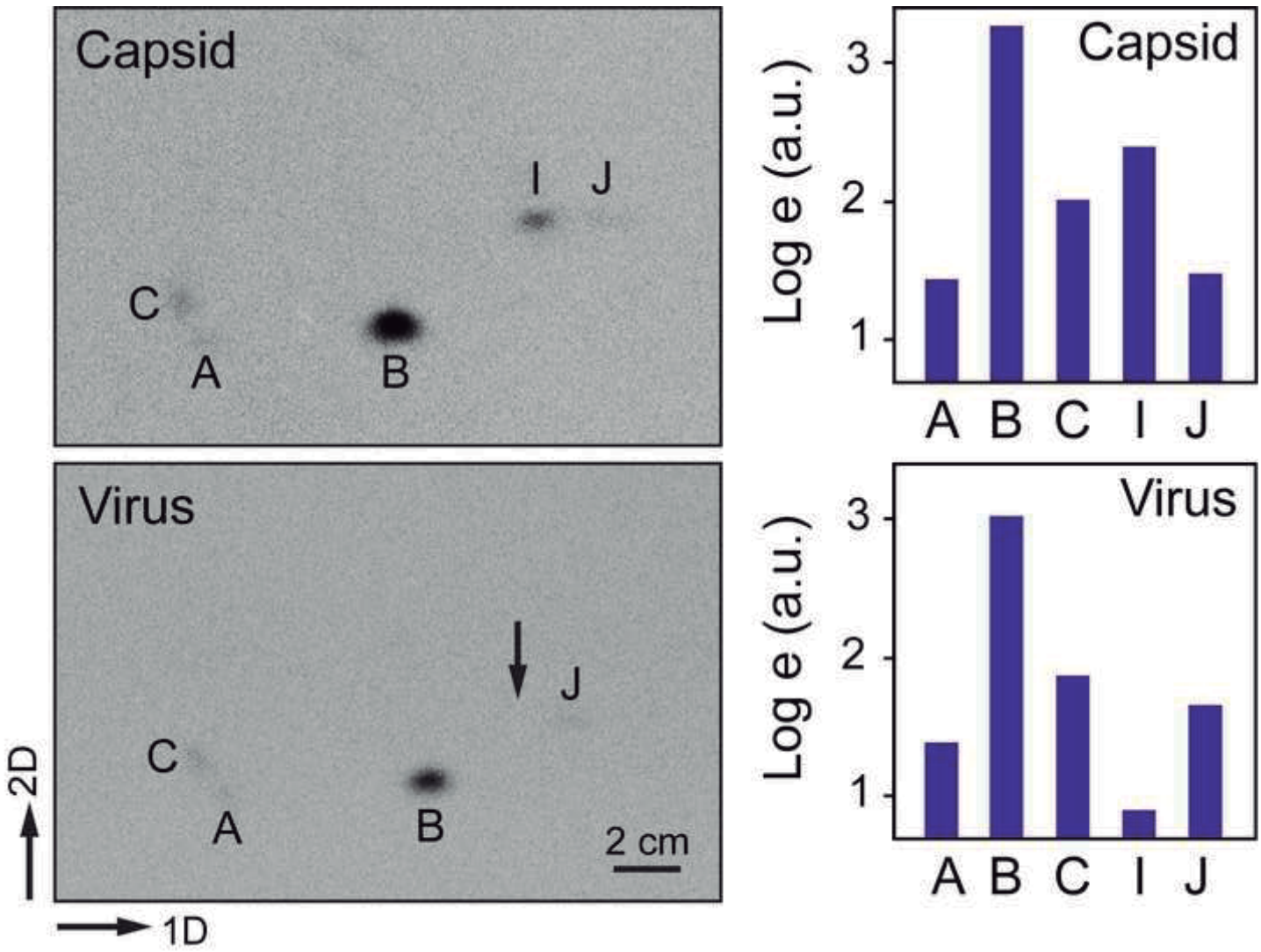

Figure 7
Click here to download high resolution image